MOLECULAR AND CELLULAR BIOLOGY, July 2009, p. 3529–3543 Vol. 29, No. 13
0270-7306/09/$08.00+0 doi:10.1128/MCB.00364-09

Fbxo45 Forms a Novel Ubiquitin Ligase Complex and Is Required for Neuronal Development▽†

Toru Saiga,[1,2] Takaichi Fukuda,[3] Masaki Matsumoto,[1,2] Hirobumi Tada,[4,5] Hirotaka James Okano,[5] Hideyuki Okano,[5] and Keiichi I. Nakayama[1,2]*

Department of Molecular and Cellular Biology, Medical Institute of Bioregulation, Kyushu University, Fukuoka 812-8582, Japan[1]; CREST, Japan Science and Technology Agency, Kawaguchi, Saitama 332-0012, Japan[2]; Department of Anatomy and Neurobiology, Graduate School of Medical Sciences, Kyushu University, Fukuoka 812-8582, Japan[3]; Physiology and Neuroendocrinology, Yokohama City University Graduate School of Medicine, Yokohama 236-0004, Japan[4]; and Department of Physiology, Keio University School of Medicine, Shinjuku, Tokyo 160-8582, Japan[5]

Received 20 March 2009/Accepted 17 April 2009

Fbxo45 is an F-box protein that is restricted to the nervous system. Unlike other F-box proteins, Fbxo45 was found not to form an SCF complex as a result of an amino acid substitution in the consensus sequence for Cul1 binding. Proteomics analysis revealed that Fbxo45 specifically associates with PAM (protein associated with Myc), a RING finger-type ubiquitin ligase. Mice deficient in Fbxo45 were generated and found to die soon after birth as a result of respiratory distress. *Fbxo45*$^{-/-}$ embryos show abnormal innervation of the diaphragm, impaired synapse formation at neuromuscular junctions, and aberrant development of axon fiber tracts in the brain. Similar defects are also observed in mice lacking Phr1 (mouse ortholog of PAM), suggesting that Fbxo45 and Phr1 function in the same pathway. In addition, neuronal migration was impaired in *Fbxo45*$^{-/-}$ mice. These results suggest that Fbxo45 forms a novel Fbxo45-PAM ubiquitin ligase complex that plays an important role in neural development.

Ubiquitin-dependent proteolysis is indispensable for various biological processes (3, 40). Protein ubiquitylation is mediated by several enzymes that act in concert, with a ubiquitin ligase (E3) playing a key role in substrate recognition (14). E3 enzymes contain specific structural motifs that mediate recruitment of a ubiquitin-conjugating enzyme (E2), with these motifs including HECT, RING finger, U-box, and PHD finger domains (30). The SCF complex consists of Skp1 (adaptor subunit), Cul1 (scaffold subunit), an F-box protein (substrate recognition subunit), and Rbx1 (also known as Roc1 or Hrt1; RING finger-containing subunit). Whereas Skp1, Cul1, and Rbx1 are common to all SCF complexes, the F-box protein is variable (with ~70 such proteins having been identified in humans) and confers substrate specificity.

Fbxo45 is an F-box protein that was originally isolated as an estrogen-induced protein (47). Human and mouse Fbxo45 genes comprise three exons and possess several consensus binding sequences for the estrogen receptor in the promoter region. Fbxo45 mRNA is rapidly induced on exposure of MCF-7 cells to 17β-estradiol (47). FSN-1, the *Caenorhabditis elegans* ortholog of Fbxo45, binds to RPM-1 (regulator of presynaptic morphology 1) together with CUL-1 and SKR-1, the *C. elegans* orthologs of mammalian Cul1 and Skp1, respectively (21, 46). RPM-1 belongs to an evolutionarily conserved family of proteins (the PHR family) that include Highwire (HIW) (*Drosophila melanogaster*), Esrom (*Danio rerio*), Phr1 (*Mus musculus*), and protein associated with Myc (PAM) (*Homo sapiens*), each of which contains a RING-finger domain that is required for its E3 activity (7, 20, 21, 27, 44). Complete loss of function of *fsn-1* in *C. elegans* results in defects that are characterized by the simultaneous presence of overdeveloped and underdeveloped neuromuscular junctions (NMJs) and which are similar to, but not as pronounced as, those observed in *rpm-1*$^{-/-}$ mutants. These genetic findings support the notion that the functions of FSN-1 and RPM-1 are partially overlapping (21).

Although PHR family members interact with many potential targets (11, 24, 26, 31), genetic data have shown that one key substrate of RPM-1 and HIW is the mitogen-activated protein kinase kinase kinase known as DLK (dual leucine zipper kinase) in *C. elegans* and known as Wallenda in *D. melanogaster*, respectively. The abundance of this kinase is increased in *rpm-1* or *hiw* mutants, and synaptic defects in the mutant worms and flies are suppressed by a loss of DLK or Wallenda. Furthermore, an increase in the level of DLK or Wallenda is sufficient to phenocopy the synaptic defects of the *rpm-1* or *hiw* mutants (5, 27). PAM has also been shown to catalyze the ubiquitylation of tuberin (TSC2) and to regulate signaling by mTOR (mammalian target of rapamycin) in human cells (12).

To elucidate the physiological functions of Fbxo45 in mammals, we have now generated mice deficient in this protein. Analysis of the mutant mice revealed that Fbxo45 is required for normal neuromuscular synaptogenesis, axon pathfinding, and neuronal migration. Moreover, we found that Fbxo45 does not form an authentic SCF complex as a result of an amino acid substitution in the F-box domain, and we identified PAM as a binding partner of Fbxo45. The phenotype of *Fbxo45*$^{-/-}$

* Corresponding author. Mailing address: Department of Molecular and Cellular Biology, Medical Institute of Bioregulation, Kyushu University, 3-1-1 Maidashi, Higashi-ku, Fukuoka, Fukuoka 812-8582, Japan. Phone: 81-92-642-6815. Fax: 81-92-642-6819. E-mail: nakayak1@bioreg.kyushu-u.ac.jp.

† Supplemental material for this article may be found at http://mcb.asm.org/.

▽ Published ahead of print on 27 April 2009.

mice was found to be similar to that of *Phr1*$^{-/-}$ mice, especially with regard to the defects of neuromuscular synapse formation and of axon navigation. Our results indicate that three fundamental processes of neural development—axonal projection, synapse formation, and neuronal migration—may be linked by a common machinery consisting of the Fbxo45-Phr1 complex.

MATERIALS AND METHODS

Construction of an Fbxo45 targeting vector and generation of Fbxo45$^{-/-}$ mice. Genomic DNA corresponding to the *Fbxo45* locus was isolated from E14 mouse embryonic stem (ES) cells by PCR using of LA-*Taq* polymerase (Takara). The targeting vector was constructed by replacing a 1.0-kb fragment of the genomic DNA containing exon 1 of *Fbxo45* with internal ribosome entry site (IRES)-*lacZ* and PGK-*neo*-poly(A)-loxP cassettes. The vector thus contained 6.3- and 1.4-kb regions of homology located 5′ and 3′, respectively, relative to IRES-*lacZ* and the neomycin resistance gene (*neo*). A diphtheria toxin A cassette was ligated at the 3′ end of the targeting construct. The maintenance, transfection, and selection of ES cells were performed as described previously (28). The recombination event was confirmed by Southern blot analysis with a 0.5-kb fragment of genomic DNA that flanked the 3′ homology region (see Fig. 3). The expected sizes of hybridizing fragments after digestion of genomic DNA with BglII and SpeI were 7.6 and 5.6 kb for the wild-type and mutant *Fbxo45* alleles, respectively. Mutant ES cells were microinjected into C57BL/6 mouse blastocysts, and the resulting male chimeras were mated with C57BL/6 females. Germ line transmission of the mutant allele was confirmed by Southern blot analysis. Heterozygous offspring were backcrossed for 12 generations to C57BL/6 mice and were then intercrossed to produce homozygous mutant animals. For genotyping of embryos, DNA was extracted from the yolk sac or tail at embryonic day 13.5 (E13.5) to E18.5 and was analyzed by PCR with the primers PJL (5′-TGC TAAAGCGCATGCTCCAGACTG-3′), TS92 (5′-GGTTTCCCATCATTCATT TTCAGC-3′), and TS93 (5′-GCCTTTTGTTTGTTTGTTTGGG-3′). All mouse experiments were approved by the animal ethics committee of Kyushu University.

Antibodies. Polyclonal anti-Rbx1 was generated in rabbits by injection with full-length recombinant human Rbx1 produced in *Escherichia coli*. Polyclonal anti-Fbxo45, anti-DLK, and anti-ALK were kindly provided by H. Okano (Keio University), S. Ohno (Yokohama City University), and T. Yamamoto (Tokyo University), respectively. Polyclonal antisynaptophysin and anti-Cul1 were obtained from Zymed; monoclonal anti-Skp1, anti-Hsp70, and anti-Hsp90 were from BD Transduction Laboratories; polyclonal anti-phospho-p38 was from Promega; polyclonal anti-extracellular signal-regulated kinase (anti-ERK), anti-phospho-ERK, anti-c-Jun NH_2-terminal kinase (anti-JNK), anti-phospho-JNK, anti-c-Jun, anti-phospho-c-Jun, and anti-TSC2 were from Cell Signaling; polyclonal antineurofilaments, monoclonal anti-FLAG (M2), and monoclonal anti-βIII-tubulin were from Sigma; monoclonal anti-hemagglutinin epitope (anti-HA) (HA11) was from Covance; polyclonal anticalretinin and anti-choline acetyltransferase were from Chemicon; polyclonal anti-LZK was from ABGENT; and monoclonal anti-Isl1 was from Developmental Studies Hybridoma Bank. Alexa 546-conjugated phalloidin and Alexa 594-conjugated α-bungarotoxin were obtained from Molecular Probes.

Preparation of tissue lysates and immunoblot analysis. Frozen tissues were cut into small pieces and then homogenized for 5 min in an ice-cold solution containing 50 mM Tris-HCl (pH 7.5), 0.25 M sucrose, 1 mM EDTA, aprotinin (10 μg/ml), leupeptin (10 μg/ml), and 1 mM phenylmethylsulfonyl fluoride. The homogenate was diluted with an equal volume of 2× radioimmunoprecipitation assay buffer (0.3 M NaCl, 20 mM Tris-HCl [pH 7.5], 2% Nonidet P-40, 0.2% sodium deoxycholate, 0.2% sodium dodecyl sulfate [SDS], aprotinin [10 μg/ml], leupeptin [10 μg/ml], 1 mM phenylmethylsulfonyl fluoride), incubated on ice for 15 min, and centrifuged at 15,000 × *g* for 15 min at 4°C. The resulting supernatant (60 μg of protein) was then subjected to immunoblot analysis as described previously (36).

Histological analysis. Tissue was fixed with 4% paraformaldehyde in phosphate-buffered saline (PBS), embedded in paraffin, and sectioned at a thickness of 5 μm. Hematoxylin-eosin staining was performed as described previously (29). For immunohistofluorescence analysis, samples were fixed with 4% paraformaldehyde in PBS, embedded in OCT compound (Tissue Tek), and sectioned with a cryostat at a thickness of 5 μm. Immunohistofluorescence staining was then performed as described previously (29). Immune complexes were detected with secondary antibodies labeled with Alexa 546 or Alexa 488 (Molecular Probes), each at a dilution of 1:2,000. The specimens were examined with a fluorescence microscope, Eclipse E800 (Nikon) or Radiance2000 (Bio-Rad), and photographed. For whole-mount staining of nerves, embryos were killed, eviscerated, fixed for 1 h with 2% paraformaldehyde in PBS, and washed with 0.1 M glycine in PBS. Tissue was then dissected, permeabilized overnight at 4°C with 0.5% Triton X-100 in PBS containing bovine serum albumin (10 mg/ml), and incubated overnight at 4°C with rabbit antibodies to synaptophysin and to neurofilaments in PBS containing bovine serum albumin (10 mg/ml). It was then washed three times for 20 min with PBS, incubated for 2 h at room temperature with Alexa 488-conjugated goat antibodies to rabbit immunoglobulin G (Molecular Probes), washed again, and mounted between coverslips. For simultaneous detection of acetylcholine receptors (AChRs) and nerve terminals, tissue was stained with Alexa 594-conjugated α-bungarotoxin and antisynaptophysin, washed, and then incubated with Alexa 488-conjugated goat antibodies to rabbit immunoglobulin G.

Skeletal staining. Skeletal staining was performed as described previously (37).

Neuronal cell culture. Dissociated primary neuronal cultures were prepared from the cerebral cortex of *Fbxo45*$^{-/-}$ mouse embryos and their wild-type littermates at E18.5. The cells were maintained in Neurobasal medium (Gibco) supplemented with B27, penicillin, streptomycin, and L-glutamine.

Analysis of cortical neurogenesis. Pregnant mice were injected intraperitoneally with 5-bromo-2′-deoxyuridine (BrdU) (50 mg per kilogram of body weight) at E14.5, and embryos were dissected and fixed at E18.5. Sections were prepared and stained to detect BrdU-positive nuclei with the use of a BrdU in-situ detection kit (BD Transduction Laboratories) and Alexa 546-conjugated streptavidin (Invitrogen).

Plasmids, transfection, and immunoprecipitation. The plasmids p3×FLAG-Fbxo45 (mouse) and pcDNA3-FLAG-PAM (human) were kindly provided by H. Okano (Keio University) and T. Patel (Loyola University), respectively. Complementary DNAs encoding Fbxw2 tagged with three copies of the FLAG epitope (3×FLAG-Fbxw2) (mouse), Fbxw2 tagged with HA (HA-Fbxw2) (mouse), 3×FLAG-Skp2 (human), HA-Skp2 (mouse), HA-Fbxo45 (mouse), mouse Fbxo45 deletion mutants tagged at their NH_2 termini with HA, and human PAM deletion mutants (R2, R3, R4, R5, and R8) tagged at their NH_2 termini with 3×FLAG were subcloned into pcDNA3 (Invitrogen). Human PAM deletion mutants R1, R6, and R7 were subcloned into p3×FLAG-CMV 7.1 (Sigma). HEK293T cells were transfected with expression plasmids by the calcium phosphate method and were cultured for 48 h before analysis. They were then collected, lysed in a solution containing 0.5% Triton X-100, and subjected to immunoprecipitation with anti-FLAG as described previously (13).

Cycloheximide chase analysis. HEK293T cells were transfected with the use of the FuGene 6 reagent (Roche). After 24 h, the cells were incubated with cycloheximide (50 μg/ml) for 0 to 9 h and then subjected to immunoblot analysis.

Analysis of Fbxo45-binding proteins. HEK293T cells transiently expressing 3×FLAG-tagged Fbxo45 or mock-transfected cells were lysed in a solution containing 50 mM Tris-HCl (pH 7.4), 150 mM NaCl, 0.5% Triton X-100, aprotinin (10 μg/ml), leupeptin (10 μg/ml), 10 mM iodoacetamide, 1 mM phenylmethylsulfonyl fluoride, 400 μM Na_3VO_4, 400 μM EDTA, 10 mM NaF, and 10 mM sodium pyrophosphate (buffer A). The lysate was centrifuged at 16,000 × *g* for 10 min at 4°C, and the resulting supernatant was applied to a column of Sepharose CL4B (GE Healthcare) conjugated with anti-FLAG (M2). The column was washed with buffer A, after which bound proteins were eluted with the 3×FLAG peptide (200 μg/ml), concentrated by precipitation with trichloroacetic acid, fractionated by SDS-polyacrylamide gel electrophoresis (PAGE), and stained with Coomassie brilliant blue G250. Protein bands were excised from the stained gel and washed, and stain was removed with acetonitrile. The proteins were reduced with 10 mM dithiothreitol, alkylated with 55 mM iodoacetamide, and digested for 16 h at 37°C with sequence-grade trypsin (Promega). The resulting peptides were sequentially extracted from the gel with 0.1% trifluoroacetic acid (TFA) in 2% acetonitrile, 0.1% TFA in 33% acetonitrile, and 0.1% TFA in 70% acetonitrile. The combined extracts were evaporated, and the residue was dissolved with 0.1% TFA in 2% acetonitrile.

Liquid chromatography and tandem mass spectrometry (LC-MS/MS) and database searching. Peptides were subjected to chromatography on a C_{18} column (0.2 mm by 5 cm; L-column) with a high-performance liquid chromatography system (Magic 2002; Michrom BioResources) that was directly coupled to an ion-trap mass spectrometer (LCQ-Deca; Finnigan) equipped with a nano-LC electrospray ionization source (AMR). Collision-induced dissociation (CID) spectra were acquired automatically in the data-dependent scan mode with the

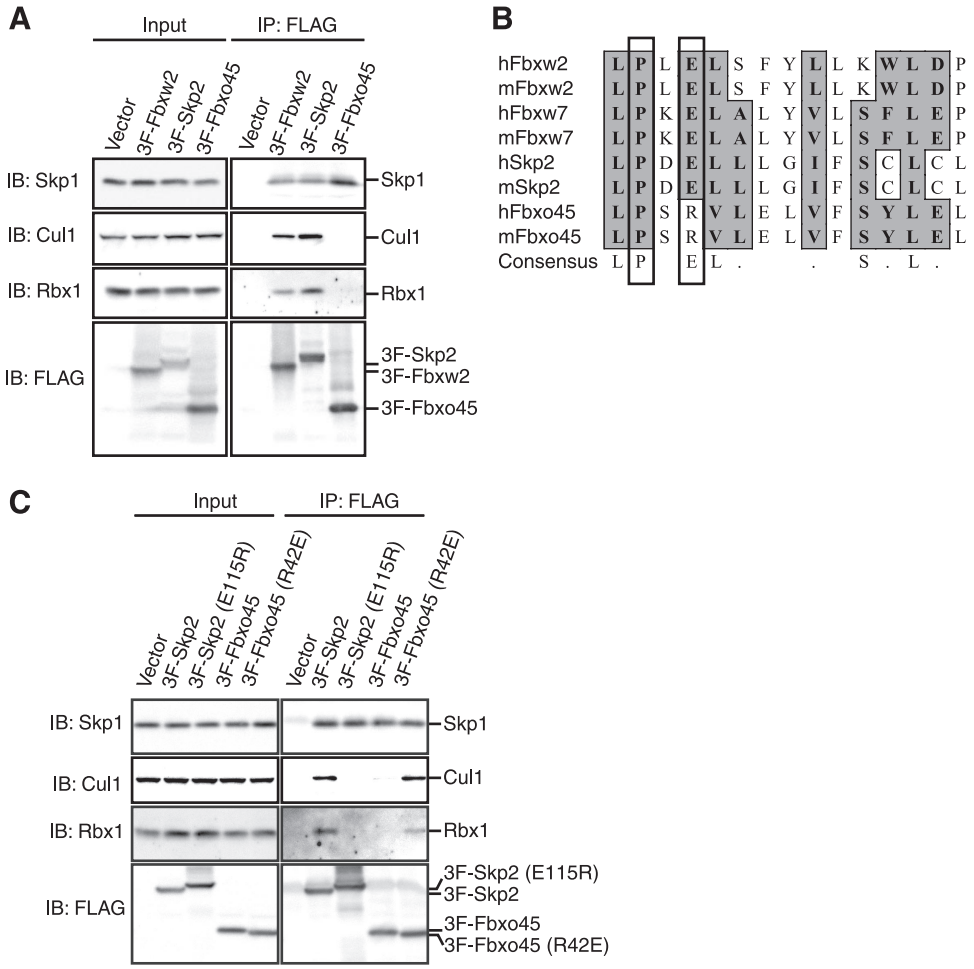

FIG. 1. Fbxo45 does not form a canonical SCF complex due to an amino acid substitution in the F-box domain. (A) Lysates of HEK293T cells expressing 3×FLAG (3F)-tagged Fbxw2, Skp2, or Fbxo45 were subjected to immunoprecipitation (IP) with anti-FLAG, and the resulting precipitates, as well as the original cell lysates (Input), were subjected to immunoblot analysis (IB) with antibodies to the indicated proteins. (B) Clustal W alignment of the F-box domains of various human (h) or mouse (m) F-box proteins. Conserved residues are shaded, and residues thought to be important for interaction with Cul1 are boxed. (C) Lysates of HEK293T cells expressing 3×FLAG-tagged Skp2, Skp2(E115R), Fbxo45, or Fbxo45(R42E) were subjected to immunoprecipitation with anti-FLAG, and the resulting precipitates and original cell lysates were subjected to immunoblot analysis with antibodies to the indicated proteins.

dynamic exclusion option. Uninterpretable CID spectra were compared with human entries in the International Protein Index (European Bioinformatics Institute) with the use of the MASCOT algorithm. Assigned high-scoring peptide sequences were manually confirmed by comparison with the corresponding CID spectra.

RESULTS

Fbxo45 does not form an SCF complex as a result of an amino acid substitution in the F-box domain. Given that most, but not all, known F-box proteins form an SCF complex with Skp1, Cul1, and Rbx1 (4, 17, 30), we examined whether Fbxo45 is able to form such a complex. Various F-box proteins tagged 3×FLAG were expressed in HEK293T cells, immunoprecipitated with antibodies to FLAG, and subjected to immunoblot analysis with anti-Skp1, anti-Cul1, and anti-Rbx1 (Fig. 1A). Fbxw2 and Skp2 (also known as Fbxl1) bound to endogenous Skp1, Cul1, and Rbx1, whereas Fbxo45 interacted with Skp1 but not with Cul1 and Rbx1. These data suggested that Fbxo45 does not form an authentic SCF complex.

The crystal structure of human SCF^{Skp2} shows that the F-box domain of Skp2 interacts not only with Skp1 but also with Cul1 (49). The Cul1-Skp2 interaction appears to be mediated by two amino acid residues, Pro^{113} and Glu^{115}, in the F-box domain of Skp2. In the loop region (amino acids 113 to 116) of Skp2, which forms the binding interface with Cul1, Pro^{113} participates in a hydrophobic interaction with Thr^{54} of Cul1 whereas Glu^{115} forms a hydrogen bond and a salt bridge with Tyr^{139} and His^{143}, respectively, of Cul1. In particular, the electrostatic interaction between the negatively charged Glu^{115} and the positively charged His^{143} appears key to the interaction between Skp2 and Cul1 (18). Alignment of the amino acid sequences of various F-box proteins (Fig. 1B) revealed that Pro^{113} and Glu^{115} of Skp2 are conserved among all such proteins examined with the exception of Fbxo45, in which the negatively charged Glu is replaced with positively charged Arg (Arg^{42}). A repulsive force between positively charged residues, Arg^{42} of Fbxo45 and His^{143} of Cul1, thus likely inhibits the

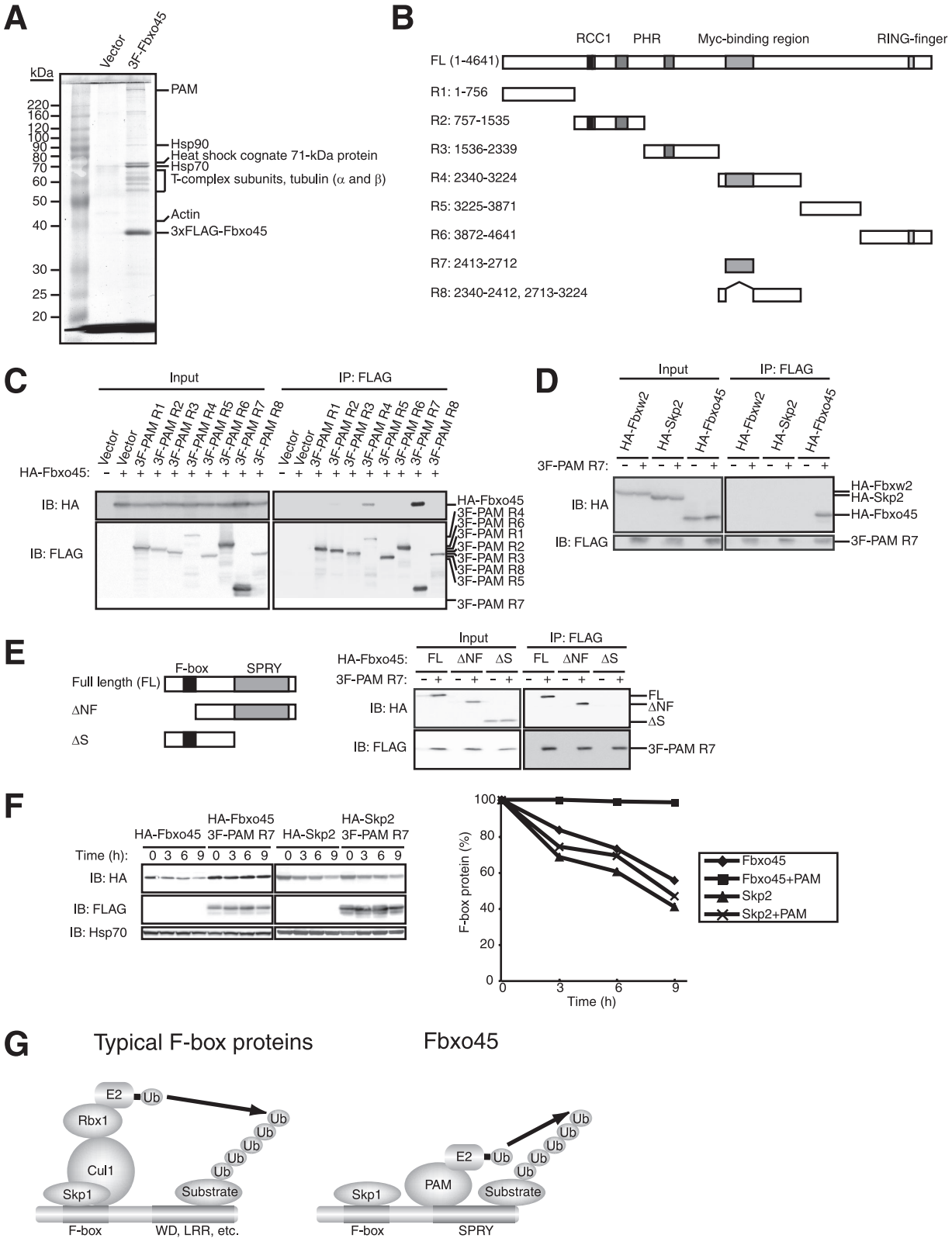

FIG. 2. Identification of PAM as a protein that interacts with Fbxo45. (A) Lysates of HEK293T cells expressing 3×FLAG-tagged Fbxo45 were subjected to immunoprecipitation with anti-FLAG, and the resulting precipitates were subjected to SDS-PAGE and staining with Coomassie blue. Proteins identified by LC-MS/MS are indicated. (B) Schematic representation of deletion mutants of human PAM. FL, full length. (C) Lysates of HEK293T cells expressing HA-tagged Fbxo45 and the 3×FLAG-tagged deletion mutants of PAM shown in panel B were subjected to immunoprecipitation (IP) with anti-FLAG, and the resulting precipitates, as well as the original cell lysates, were subjected to immunoblot (IB) analysis with antibodies to HA and to FLAG. (D) Lysates of HEK293T cells expressing HA-tagged Fbxw2, Skp2, or Fbxo45 together with the 3×FLAG-

binding of Fbxo45 to Cul1. Indeed, replacement of Arg^{42} of Fbxo45 with Glu (R42E) conferred on Fbxo45 the ability to bind to Cul1 and Rbx1 (Fig. 1C). Conversely, a Skp2 mutant (E115R) in which Glu^{115} is replaced with Arg did not bind to Cul1 and Rbx1 (Fig. 1C). We therefore conclude that an amino acid substitution in the F-box domain of Fbxo45 prevents the interaction of Fbxo45 with Cul1 and Rbx1.

PAM is a binding partner of Fbxo45. Given that Fbxo45 is not able to associate with Cul1 and Rbx1, we hypothesized that it might interact with another RING-finger protein. We thus adopted a proteomics approach to identify proteins that bind to Fbxo45. An expression plasmid encoding 3×FLAG-tagged Fbxo45 was introduced into HEK293T cells, and immunoprecipitates prepared from cell lysates with anti-FLAG were subjected to SDS-PAGE. An ~500-kDa protein was thus found to interact specifically with Fbxo45 (Fig. 2A) and was identified as PAM, a RING finger-type ubiquitin ligase, by LC-MS/MS. In addition, Skp1, but not Cul1 and Rbx1, was identified in the immunoprecipitates by LC-MS/MS analysis (data not shown), consistent with the results of coimmunoprecipitation experiments.

To determine the region of PAM that is responsible for binding to Fbxo45, we generated a series of deletion mutants (R1 to R6) of PAM (Fig. 2B) and tested their ability to bind to HA-tagged Fbxo45 by coimmunoprecipitation analysis in HEK293T cells. Only the R4 deletion mutant, which contains the Myc-binding region, was found to interact with Fbxo45 (Fig. 2C). We next generated a mutant comprising the Myc-binding region alone (R7) and its reciprocal R4-based mutant (R8). The R7 mutant interacted with Fbxo45 to a great extent, whereas the R8 mutant showed no detectable association, indicating that the Myc-binding region of PAM is sufficient for binding to Fbxo45. The interaction of the Myc-binding region of PAM with Fbxo45 was shown to be specific in that no such interaction was apparent with Fbxw2 or Skp2 (Fig. 2D). We also examined which domain of Fbxo45 is responsible for binding to PAM (Fig. 2E). An NH_2-terminal deletion mutant lacking the F-box domain retained the ability to interact with PAM, whereas a COOH-terminal deletion mutant lacking the SPRY domain did not. These data thus suggested that the SPRY domain of Fbxo45 mediates the interaction with PAM.

Interaction with the Myc-binding region of PAM stabilizes Fbxo45. We observed that the abundance of full-length Fbxo45 and the NH_2-terminal deletion mutant of Fbxo45 but not that of the COOH-terminal deletion mutant was greater when these proteins were coexpressed with the Myc-binding region of PAM (Fig. 2E). To determine whether this phenomenon might be attributable to stabilization of Fbxo45 by PAM, we transfected HEK293T cells with a vector for HA-tagged Fbxo45 or HA-tagged Skp2 (negative control) in the absence or presence of a vector for the 3×FLAG-tagged R7 deletion mutant of PAM. A cycloheximide chase experiment revealed that Fbxo45 was more stable in cells coexpressing the Myc-binding region of PAM than in those expressing Fbxo45 alone whereas the stability of Skp2 was unaffected by coexpression of the Myc-binding region of PAM (Fig. 2F). The stability of PAM did not appear to be affected by Fbxo45 (data not shown). These results thus support the notion that Fbxo45 and PAM form a novel complex that is independent of Cul1 and Rbx1 (Fig. 2G).

Generation of mice lacking Fbxo45. To elucidate the physiological functions of Fbxo45, we generated mice deficient in this protein. The Fbxo45 gene was disrupted in mouse ES cells by replacement of exon 1 with IRES-*lacZ* and PGK-*neo*-poly(A)-loxP cassettes (Fig. 3A and B). Mice heterozygous for the *Fbxo45* mutant allele were healthy, fertile, and phenotypically indistinguishable from wild-type littermates, although the abundance of Fbxo45 in tissues of the mutant mice was about half of that in those of wild-type animals (Fig. 3C). In contrast, no adult homozygous mutants were obtained from heterozygote crosses (see Table S1 in the supplemental material). $Fbxo45^{-/-}$ embryos were recovered at the expected Mendelian ratio until E17.5 to E18.5, suggesting that the homozygous mutation is not embryonic lethal. Immunoblot analysis revealed that Fbxo45 was exclusively expressed in neuronal tissues, including the cerebrum and medulla oblongata in wild-type mice, whereas it was not detectable in $Fbxo45^{-/-}$ mice (Fig. 3D). These data suggested that Fbxo45 might play an important role in neural development.

Homozygous mutant newborns were found to die within 30 min after birth and were readily distinguished by their characteristic tucked position, pale color (Fig. 3E), and absence of spontaneous movement. The $Fbxo45^{-/-}$ mice also exhibited skeletal deformities, such as kyphosis (Fig. 3F). At E16.5, the homozygous mutants had a beating heart, and all internal organs appeared intact and appropriately positioned (see Fig. S1 in the supplemental material). Pulmonary alveoli of $Fbxo45^{-/-}$ newborns did not expand, although all components of lung tissue appeared normal (Fig. 3G and H). Together with the neuropathological anomalies described below, these obser-

tagged R7 deletion mutant of PAM were subjected to immunoprecipitation with anti-FLAG, and the resulting precipitates, as well as the original cell lysates, were subjected to immunoblot analysis with antibodies to HA or to FLAG. (E) Lysates of HEK293T cells expressing the HA-tagged deletion mutants of mouse Fbxo45 indicated on the left and the 3×FLAG-tagged R7 deletion mutant of PAM were subjected to immunoprecipitation with anti-FLAG, and the resulting precipitates, as well as the original cell lysates, were subjected to immunoblot analysis with antibodies to HA or to FLAG. (F) HEK293T cells expressing HA-tagged Fbxo45 (or HA-Skp2 as a negative control) with or without the 3×FLAG (3F)-tagged R7 deletion mutant of PAM (residues 2413 to 2712) were treated with cycloheximide for the indicated times, after which cell lysates were subjected to immunoblot analysis with antibodies to HA, to FLAG, or to Hsp70 (loading control). The band intensities of HA-tagged Fbxo45 or Skp2 in the upper panels were quantified relative to the corresponding values for time zero (bottom panel). (G) Model for formation of an Fbxo45-PAM complex. In typical F-box proteins, the F-box domain interacts not only with Skp1 but also with Cul1, resulting in the formation of an SCF complex. In contrast, an amino acid substitution in the F-box domain of Fbxo45 interferes with the binding to Cul1 and thereby prevents formation of an SCF complex. Instead, the SPRY domain of Fbxo45 binds directly to PAM, resulting in the formation of an Fbxo45-PAM complex. Ub, ubiquitin.

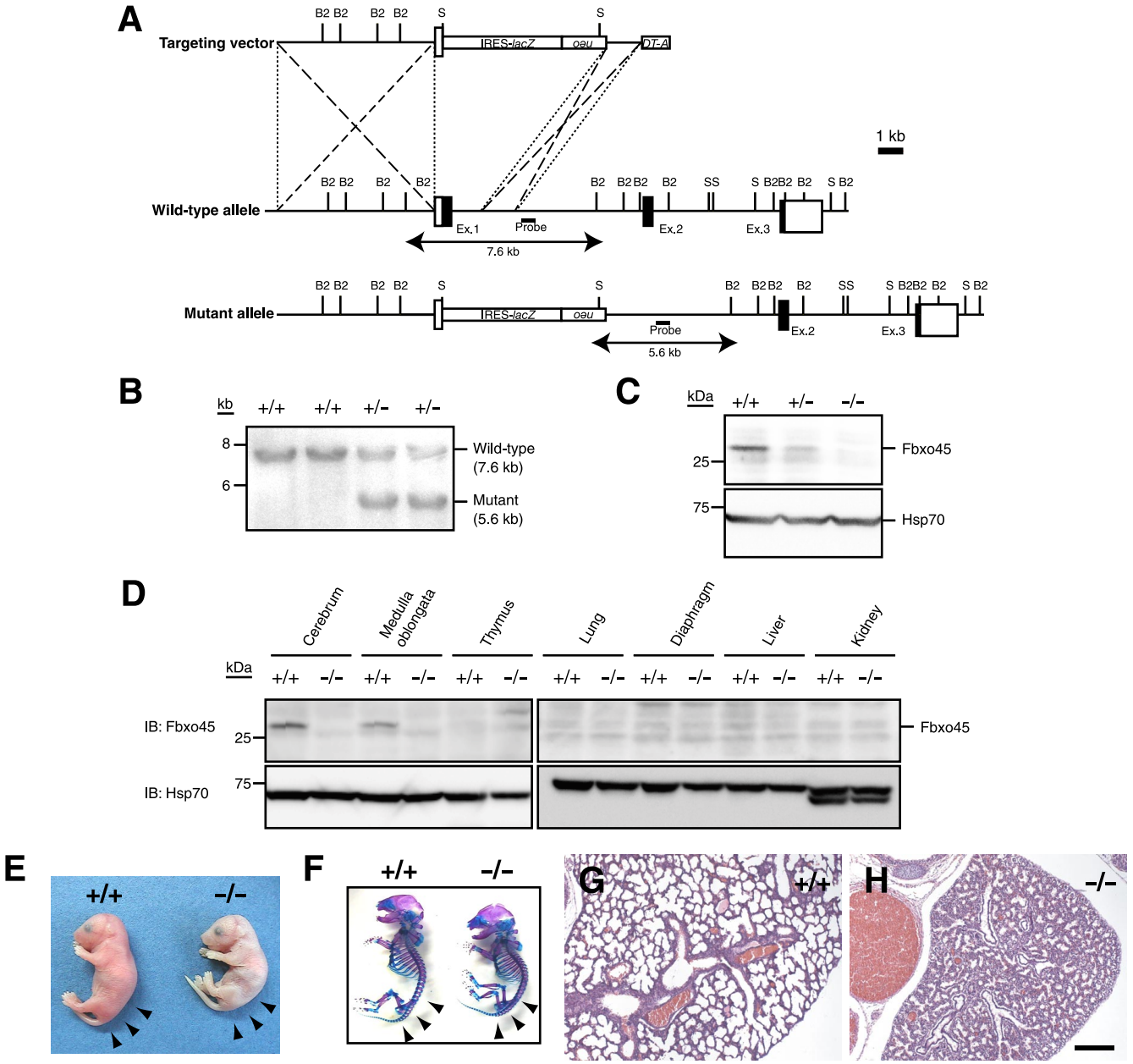

FIG. 3. Targeted disruption of *Fbxo45*. (A) Schematic representation of the wild-type *Fbxo45* locus, the targeting vector, and the mutant allele after homologous recombination. A 1.0-kb genomic fragment including exon 1 of *Fbxo45*, which encodes the F-box domain, was replaced by IRES-*lacZ* and PGK-*neo*-poly(A)-loxP cassettes. Exon (Ex.) 2 and the coding portions of exons 1 and 3 are depicted by filled boxes, with the open boxes indicating the noncoding portions of exons 1 and 3. A genomic fragment used as a probe for Southern blot analysis is shown as a solid bar. Restriction sites: B2, BglII; S, SpeI. DT-A, diphtheria toxin A cassette. (B) Southern blot analysis with the probe shown in panel A of genomic DNA isolated from the tail of adult mice and digested with BglII and SpeI. The 7.6- and 5.6-kb bands corresponding to the wild-type and mutant alleles, respectively, are indicated. The *Fbxo45* genotypes of the analyzed mice are shown above each lane. (C and D) Immunoblot analysis with anti-Fbxo45 and anti-Hsp70 (loading control) of lysates of the brain (C) or the indicated tissues (D) from mice of the indicated *Fbxo45* genotypes at postnatal day 1. (E and F) Gross appearance of newborn littermates (E) and the skeletons of E18.5 littermates (F) of the indicated *Fbxo45* genotypes. Arrowheads indicate lordotic body posture specific to *Fbxo45*$^{-/-}$ pups. (G and H) Lung sections of newborn wild-type (G) or *Fbxo45*$^{-/-}$ (H) littermates were stained with hematoxylin-eosin. The pulmonary alveoli were expanded with air only in the wild-type animal. Scale bar, 200 μm.

vations suggested that *Fbxo45* mutant mice die as a result of respiratory distress.

Loss of Fbxo45 results in innervation defects in the periphery. Given the lack of respiratory movement in neonatal *Fbxo45*$^{-/-}$ mice, we focused on the NMJs of respiratory muscles, especially those of the diaphragm. In wild-type mice, axons of the phrenic nerve exit the cervical spinal cord and contact the developing diaphragm at E12. The nerve and muscle develop together, with the nerve having formed three main branches—one extending dorsally to the crus, one innervating

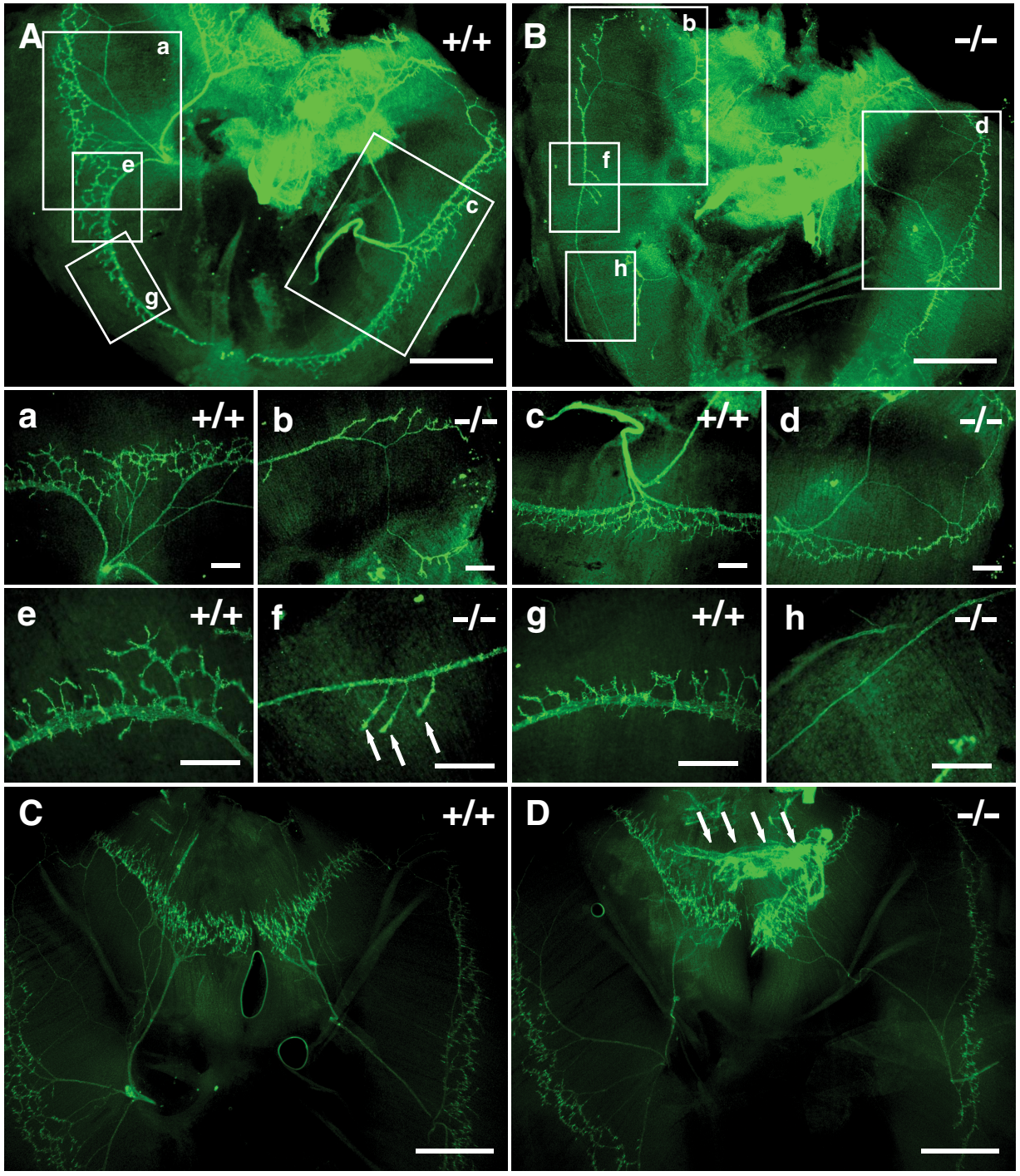

FIG. 4. Innervation defects in *Fbxo45*$^{-/-}$ mice. The diaphragm of wild-type (A and C) or *Fbxo45*$^{-/-}$ (B and D) embryos at E14.5 (A and B) or E15.5 (C and D) was subjected to whole-mount immunofluorescence staining with antibodies to neurofilaments and to synaptophysin. The boxed regions in panels A and B are shown at higher magnification in panels a through h. In wild-type embryos, the phrenic nerve reaches the diaphragm, branches, and projects both dorsally and ventrally (A). In *Fbxo45*$^{-/-}$ embryos, however, branching and projection of the phrenic nerve are impaired (B). Furthermore, the phrenic nerve sometimes branches toward the inside in *Fbxo45*$^{-/-}$ mice (arrows in panel f), whereas it branches toward the outside of the diaphragm in wild-type embryos (a, c, e, and g). Arrows in panel D indicate excessive growth and entanglement of the right and left phrenic nerves in the mutant embryo. Scale bars, 800 μm (A to D) or 250 μm (a to h).

the dorsal portion of the diaphragm, and one innervating the ventral portion of the diaphragm—by E13 (9). Whole-mount immunostaining of the diaphragm at E14.5 or E15.5 revealed that motor innervation of the diaphragm was incomplete in *Fbxo45*$^{-/-}$ mice (Fig. 4A and B). Whereas the entire diaphragm is contacted by axons of the phrenic nerve in wild-type mice, branching and projection of the phrenic nerve in the mutant mice were substantially impaired, with axons consis-

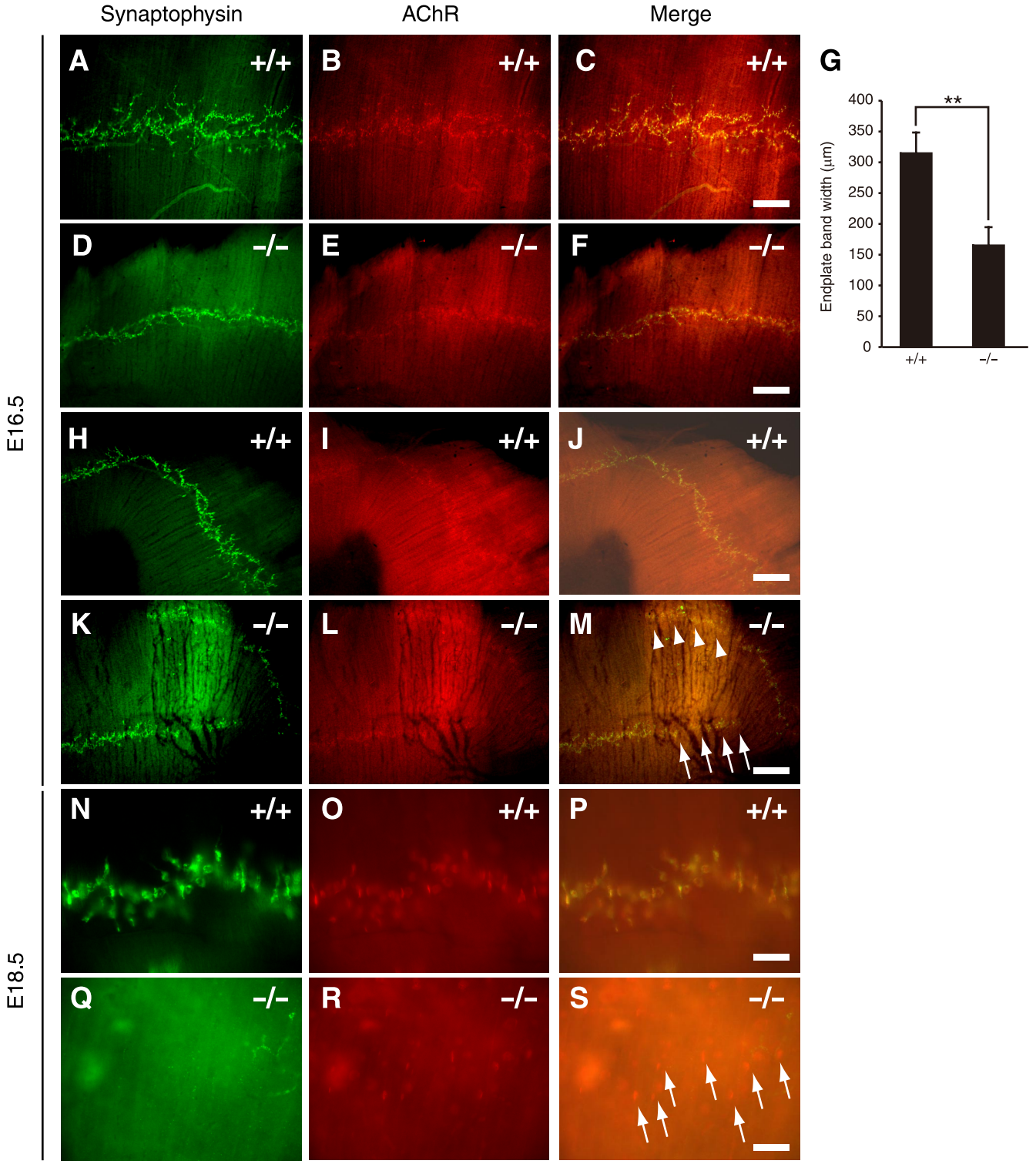

FIG. 5. Neuromuscular synapses in mice lacking Fbxo45. The diaphragm of wild-type (A, B, C, H, I, and J) or *Fbxo45*$^{-/-}$ (D, E, F, K, L, and M) embryos at E16.5 or of wild-type (N to P) or *Fbxo45*$^{-/-}$ (Q to S) embryos at E18.5 was subjected to whole-mount fluorescence staining with antisynaptophysin (for presynaptic nerve terminals) and with α-bungarotoxin (for AChRs), as indicated. Synaptophysin is colocalized with AChRs in the diaphragm of both wild-type and *Fbxo45*$^{-/-}$ embryos, indicating that NMJs are correctly connected in the mutant; however, the number of synapses is decreased in the diaphragm of *Fbxo45*$^{-/-}$ embryos (A to F). Quantification of the mean endplate bandwidth is shown in panel G. Data are means ± SEM for five embryos of each genotype. The *P* value was determined by Student's *t* test. **, $P < 0.01$. Higher-magnification views of the left portion of the pars sternalis in panel H through M reveal the formation of synapses between muscle and the left phrenic nerve, with muscle fibers having only one endplate band in their central region, in wild-type embryos. In contrast, synapses form not only between muscle and the left phrenic nerve (arrows) but also between muscle and the right phrenic nerve extending across the ventral midline (arrowheads) in *Fbxo45*$^{-/-}$ embryos. Higher-magnification views of the diaphragm also reveal an aneural region in the *Fbxo45*$^{-/-}$ embryo at E18.5 (Q to S) and the corresponding region of a wild-type embryo (N to P); arrows indicate postsynaptic differentiation in this region of the mutant. Scale bars: 200 μm (A, B, C, D, E, F, H, I, J, K, L, and M) or 50 μm (N to S).

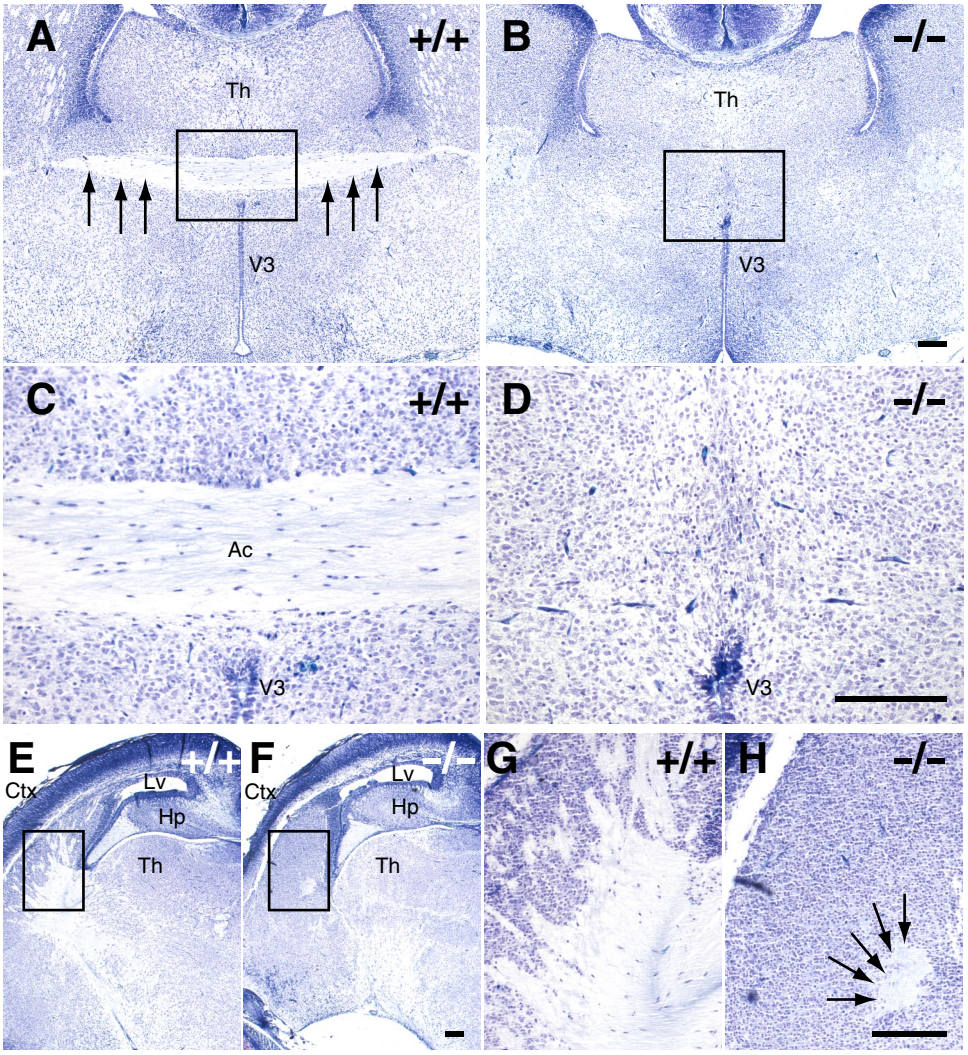

FIG. 6. Defective development of fiber tracts in *Fbxo45* mutant embryos. Coronal sections of the head portion of wild-type (A, C, E, and G) or *Fbxo45*$^{-/-}$ (B, D, F, and H) mice at E18.5 were stained with cresyl violet. Higher-magnification views of the boxed regions in panels A, B, E, and F are shown in panels C, D, G, and H, respectively. The anterior commissure (arrows in panel A) and internal capsule are apparent in the wild-type but not the *Fbxo45*$^{-/-}$ brain. In the *Fbxo45*$^{-/-}$ brain, the internal capsule is replaced by an aberrant bundle (arrows in panel H). Abbreviations: Ac, anterior commissure; Ctx, cortex; Hp, hippocampus; Lv, lateral ventricle; Th, thalamus; V3, third ventricle. Scale bars, 500 μm.

tently failing to reach the most ventral region of the diaphragm. Furthermore, branching of axons in the mutant animals was sometimes misoriented (Fig. 4B, panel f). In wild-type mice, right and left phrenic nerves innervate the right and left portions of the diaphragm, respectively, and the regions innervated by the two nerves do not overlap (Fig. 4C). In contrast, in the diaphragm of *Fbxo45*$^{-/-}$ mice, right and left phrenic nerves sometimes extended across the endplate band of the muscle and became entangled (Fig. 4D).

We next examined whether peripheral sensory projections were similarly affected by *Fbxo45* deletion. Whole-mount immunostaining revealed excessive branching of cutaneous sensory nerves in *Fbxo45*$^{-/-}$ mice at E14.5 (see Fig. S2 in the supplemental material). Axons appeared overgrown, and the nerves were defasciculated. This pattern of innervation resulted in a decrease in the areas surrounded by the sensory nerves in *Fbxo45*$^{-/-}$ mice compared with those in wild-type mice.

Aberrant patterning of neuromuscular synapses in *Fbxo45*$^{-/-}$ embryos. We next analyzed the pattern of developing neuromuscular synapses in *Fbxo45* mutants at E16.5 and E18.5. To examine the distribution of nerves and clusters of AChRs, we stained presynaptic nerve terminals and postsynaptic AChRs with antisynaptophysin and α-bungarotoxin, respectively. In wild-type mice, NMJs are confined to a central region of the muscle fiber, the endplate band, which corresponds to the region in which intramuscular nerves are located (33, 41). Although AChRs were largely clustered within the endplate band of the muscle in both wild-type (Fig. 5A to C) and mutant (Fig. 5D to F) embryos, the band of AChR clusters in *Fbxo45*$^{-/-}$ mice was much narrower than that in wild-type mice at E16.5 (Fig. 5A to F; quantified in Fig. 5G) and was

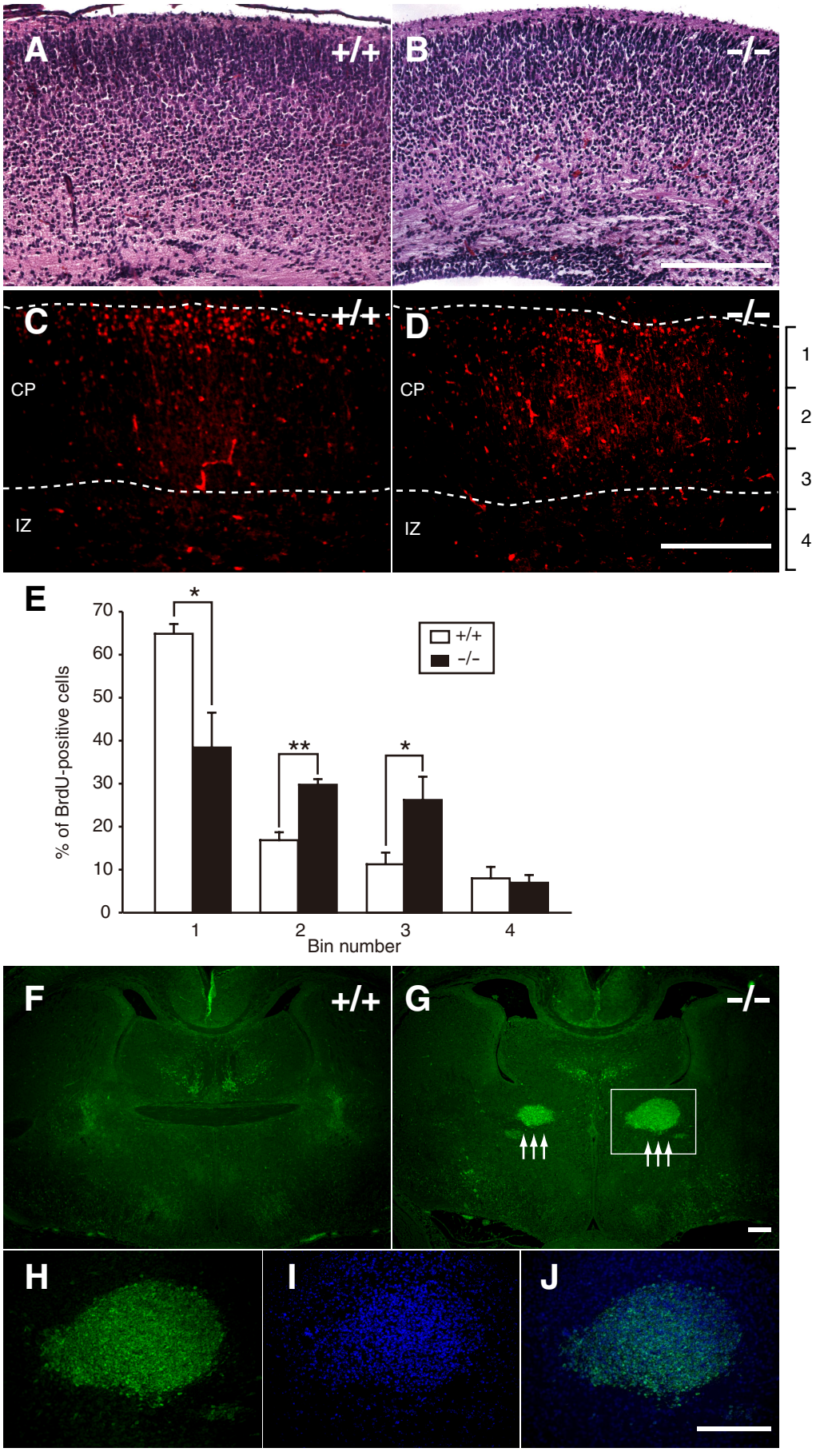
A
+/+
B
−/−
C
+/+
CP
IZ
D
−/−
CP
IZ
1
2
3
4
E
% of BrdU-positive cells
70
60
50
40
30
20
10
0
+/+
−/−
*
**
*
1
2
3
4
Bin number
F
+/+
G
−/−
H
I
J

partially aneural at E18.5 (Fig. 5N to S). Furthermore, an ectopic endplate band was formed in the region of the pars sternalis of the diaphragm in some mutant embryos. In wild-type embryos, synapses between muscle and the left phrenic nerve are formed in the left portion of the pars sternalis, with muscle fibers manifesting only one endplate band in their central portion (Fig. 5H to J). However, in the diaphragm of mutant embryos, synapses were formed not only between muscle and the left phrenic nerve but also between muscle and the right phrenic nerve extending across the ventral midline in the left portion of the pars sternalis (Fig. 5K to M). Phrenic nerves never extend across the ventral midline in wild-type mice. These results suggested that Fbxo45 plays an indispensable role in normal innervation and synaptogenesis by peripheral nerves during development.

Fbxo45 deficiency affects major axonal tracts. The widespread expression of Fbxo45 in the central nervous system, together with the innervation defects in the periphery of *Fbxo45*$^{-/-}$ mice, led us to examine the major axon tracts in the brains of mutant embryos. The brains of *Fbxo45*$^{-/-}$ embryos at E18.5 were smaller than those of wild-type mice (see Fig. S3A in the supplemental material). Histological sections revealed that the major axon tracts in the brain differed markedly between the two genotypes at E18.5. The anterior commissure was absent in *Fbxo45*$^{-/-}$ mice (Fig. 6A to D). The internal capsule was also absent, as were corticofugal and thalamocortical projections in the subcortical telencephalon (Fig. 6E to H). In contrast, the corpus callosum of mutant embryos was indistinguishable from that of wild-type embryos (see Fig. S3B and C in the supplemental material). Primary cultures of neurons prepared from the brains of *Fbxo45*$^{-/-}$ embryos at E18.5 manifested outgrowth of projections (see Fig. S4 in the supplemental material), suggesting that the loss of major axon tracts in the brains of *Fbxo45*$^{-/-}$ mice does not result from impairment of axon outgrowth. These results thus suggested that Fbxo45 is necessary for the formation of certain axonal tracts in the brain.

Cell migration defects in brains and spinal cords of *Fbxo45*$^{-/-}$ embryos. Development of the cerebral cortex normally proceeded in mutant embryos at an early stage (E14.5), as the cortical plate was formed in the preplate, splitting it into the marginal zone and the subplate. The laminated cortical structure was partly formed at postnatal day 1, and layer-specific differences in staining and cell density were prominent in the cortical plate of wild-type embryos (Fig. 7A). However, in mutant embryos, such differential patterns of different types of cells were not clearly observed (Fig. 7B). We next examined neuronal migration in *Fbxo45* mutant mice by pulse labeling with BrdU at E14.5. A large subset (65%) of labeled nuclei was located in the outermost layer of the cortical plate adjacent to the marginal zone (bin 1) in the cortex of wild-type embryos at E18.5 (Fig. 7C and E). In contrast, BrdU-labeled nuclei were more dispersed in the cortical plate of mutant embryos, with a smaller subset (38%) of these nuclei being detected in the outermost layer (Fig. 7D and E). These observations indicated that radial migration of neurons was impaired in the mutant embryos. We also examined brain sections (E18.5) stained for calretinin, a marker of cortical interneurons. Although not all interneurons express calretinin, this marker has been used routinely to reveal a large subpopulation of γ-aminobutyric acid-containing interneurons that migrate tangentially to the cortex or hippocampus (22, 45). Calretinin-positive cells accumulated abnormally in the basal telencephalon—the area in which migrating interneurons arise (23)—in the brains of *Fbxo45* mutant embryos (Fig. 7G to J). In contrast, few calretinin-positive cells were apparent in the basal telencephalon of the wild-type brain as a result of the migration of interneurons to the cortex or hippocampus (Fig. 7F).

Furthermore, development of the entire spinal cord was markedly affected by the loss of Fbxo45, as evidenced by lateral expansion of gray matter (Fig. 8A to D) and aberrant distribution of motor neurons (Fig. 8E to H). Neurons arise in the ventricular zone, located within the medial portion of the spinal cord, and migrate to their final position at the lateral edge of the cord. At brachial and lumbar levels, motor neurons are located in two regions: those that innervate limb muscle form the lateral motor column (LMC), and those that innervate the body wall form the medial motor column (MMC) (19, 42). The LMC was poorly formed and the MMC was aberrantly distributed in the spinal cords of *Fbxo45*$^{-/-}$ embryos (Fig. 8E to H). These results suggested that Fbxo45 is important for cell migration in the brain and spinal cord.

Expression of candidate targets of Fbxo45-PAM in brains of *Fbxo45*$^{-/-}$ embryos. Evolutionary considerations suggest that the Fbxo45-PAM complex might target the receptor tyrosine kinase ALK, the mitogen-activated protein kinase kinase kinase DLK, or tuberin (TSC2) for ubiquitylation-dependent proteolysis (5, 12, 21, 26, 27). We therefore examined whether these candidate proteins accumulate in the brains of *Fbxo45*$^{-/-}$ embryos. Immunoblot analysis revealed that neither the abundance of ALK nor the phosphorylation level of ERK, which functions downstream of ALK (25), differed between wild-type and *Fbxo45*$^{-/-}$ embryos (see Fig. S5A and B in the supplemental material). We also observed no difference

FIG. 7. Impaired neuronal migration in *Fbxo45*$^{-/-}$ forebrain. (A and B) Coronal sections of wild-type (A) or mutant (B) neocortex beneath bregma at postnatal day 1 were stained with hematoxylin-eosin. (C and D) BrdU was administered to pregnant mice at E14.5, the brain was isolated from wild-type (C) or *Fbxo45*$^{-/-}$ (D) embryos at E18.5, and coronal sections of the neocortex were subjected to immunofluorescence staining with anti-BrdU. (E) To quantify the distribution of BrdU-positive nuclei, the cortical plate and intermediate zone were divided into four equal bins from the pial side to the ventricular side. The number of nuclei in each bin was determined, and these are shown as percentages of the total numbers of nuclei in the cortical plate and intermediate zone. Data are means ± SEM for three embryos of each genotype. The *P* value was determined by Student's *t* test. *, $P < 0.05$; **, $P < 0.01$. (F to J) Coronal sections of the brain tissue of wild-type (F) or *Fbxo45*$^{-/-}$ (G) embryos at E18.5 were subjected to immunofluorescence staining with anticalretinin. Arrows indicate accumulation of calretinin-positive cells in the basal telencephalon of the mutant embryo. The boxed region in panel G is shown at higher magnification in panel H; staining of the same region with Hoechst 33258 is shown in panel I, and the merged image in panel J reveals colocalization of calretinin and Hoechst 33258 staining. Abbreviations: CP, cortical plate; IZ, intermediate zone. All scale bars, 200 μm.

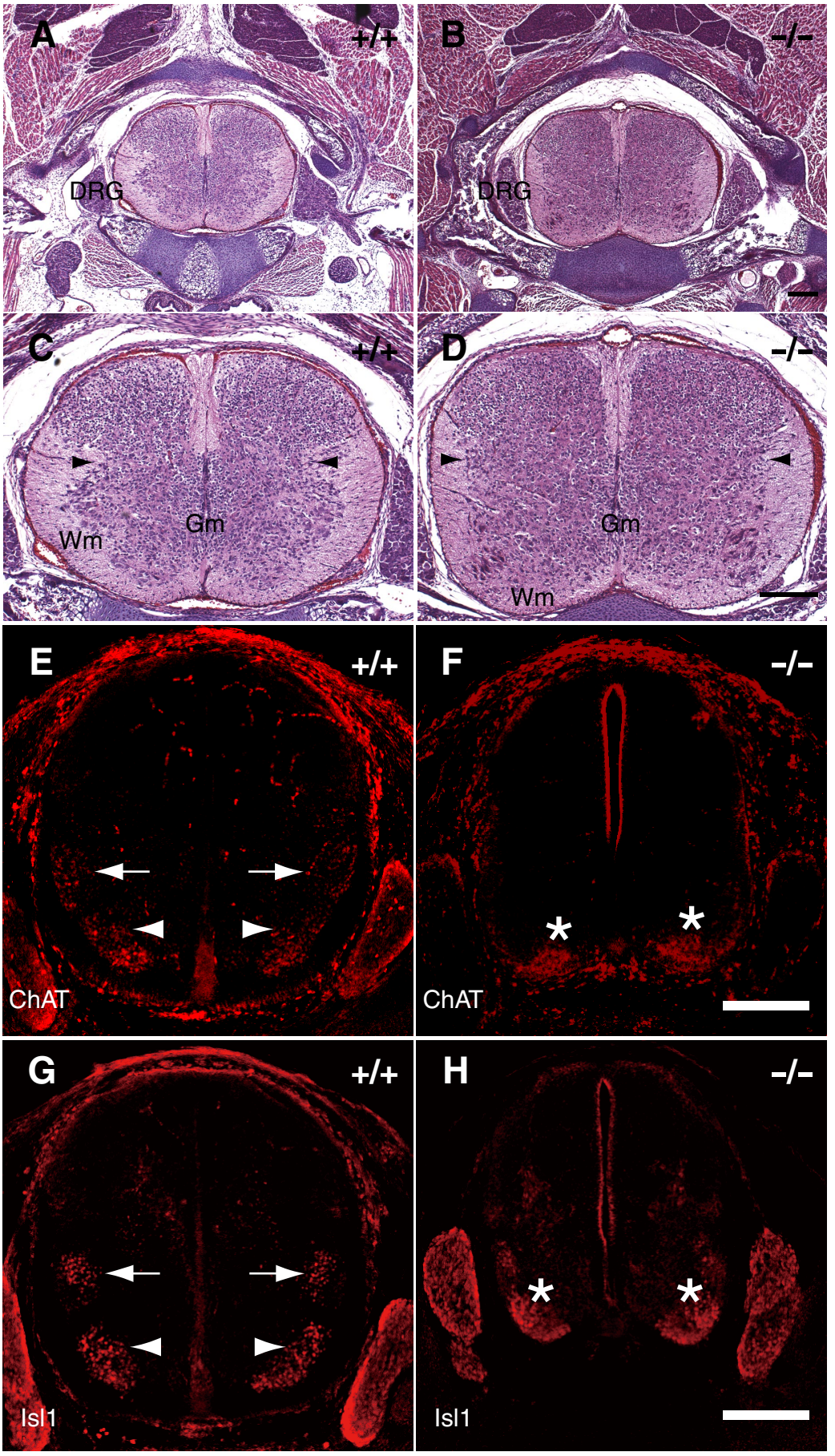
A
+/+
DRG
B
−/−
DRG
C
+/+
Wm
Gm
D
−/−
Gm
Wm
E
+/+
ChAT
F
−/−
ChAT
G
+/+
Isl1
H
−/−
Isl1

in the amounts of DLK or in the phosphorylation levels of p38 mitogen-activated protein kinase, JNK, or c-Jun, all of which function downstream of DLK (8, 15), between the two genotypes (see Fig. S5C to E in the supplemental material). In addition, the abundance of TSC2 did not appear to be affected by *Fbxo45* deletion (see Fig. S5F in the supplemental material). Finally, the abundance of LZK, the other closest mammalian homolog of DLK (32), did not appear to differ between the two genotypes (see Fig. S5G in the supplemental material). These results thus suggest that ALK, DLK, TSC2, and LZK are not targets of Fbxo45 in the brain or that other ubiquitin ligases may participate in the degradation of these proteins.

DISCUSSION

Whereas eukaryotic genomes encode hundreds of F-box proteins (10, 17), only a single F-box protein that contains a SPRY domain has been identified in worms, flies, mice, or humans (21, 43, 47). Moreover, all of these last proteins are more closely related to each other by sequence than to other F-box proteins (21, 43). We have now shown that the mammalian F box- and SPRY domain-containing protein Fbxo45 forms an atypical ubiquitin ligase complex with the RING-finger protein PAM and that Fbxo45 is required for normal development of central and peripheral neurons. Although the physical association of Fbxo45 with PAM (*H. sapiens*) and of FSN-1 with RPM-1 (*C. elegans*) is evolutionarily conserved, the composition of the mammalian Fbxo45-PAM complex appears to differ from that of the *C. elegans* FSN-1–RPM-1 complex. Our results show that mammalian Fbxo45 contains a substitution in the F-box domain for an amino acid that is conserved in other F-box proteins and that this amino acid substitution interferes with the binding of Fbxo45 to Cul1. Fbxo45 thus retains the ability to associate with Skp1 but not with Cul1 and Rbx1 (the RING finger-containing subunit of conventional SCF complexes). Instead of Rbx1, Fbxo45 interacts directly or indirectly through its SPRY domain with PAM in a manner independent both of the F-box domain of Fbxo45 and of Skp1. Fbxo45 thus appears to bind to Skp1 via its NH_2-terminal F-box domain and to PAM via its COOH-terminal SPRY domain. In contrast, *C. elegans* FSN-1 forms an SCF-like complex with SKR-1, CUL-1, and RPM-1 (21).

Our present results also reveal that the role of Fbxo45 in neural development has been conserved during evolution. However, mammalian Fbxo45 not only regulates the fine structure of synaptic connections, as does its invertebrate orthologs (21, 43), but also is required for proper neuronal migration and large-scale patterning of neuronal connectivity in the brain. The impaired branching and projection of the phrenic nerve and the partial innervation of the diaphragm apparent in *Fbxo45*$^{-/-}$ mice are indicative of functions for Fbxo45 beyond the regulation of nerve terminal morphology, such as control of the guidance of axons to their targets. Indeed, we detected a pronounced and specific loss of axon tracts throughout the central nervous system of the mutant mice, with the anterior commissure being completely absent and both thalamic and cortical axons failing to enter the subcortical telencephalon to form the internal capsule. Furthermore, neuronal migration was found to be impaired in Fbxo45-deficient embryos. These results thus suggest that Fbxo45 performs additional functions in neural development compared with its invertebrate orthologs. Consistent with this notion, the abundance of potential substrates including those targeted by invertebrate Fbxo45 orthologs—including ALK, DLK, and LZK (21, 27)—was not affected by the loss of Fbxo45 in mice, suggesting that other proteins may be targeted by Fbxo45 in mammals and that deregulation of the abundance of these proteins might be responsible for the defects in neural development observed in *Fbxo45*$^{-/-}$ mice.

Given that PAM and its orthologs Phr1 and RPM-1 are large proteins consisting of multiple functional domains (2, 11, 35, 48), these molecules are thought to perform more functions than Fbxo45 and its orthologs. In *C. elegans*, worms lacking functional FSN-1 exhibit a phenotype that is highly similar to that of *rpm-1* mutants with regard to γ-aminobutyric acid-ergic synapses but less pronounced with regard to DD motoneurons and sensory neurons (21). These differences in phenotype suggest that RPM-1 might either interact with other F-box proteins in addition to FSN-1, act as a ubiquitin ligase without an F-box partner, or perform ubiquitin-independent functions. We also found marked similarity between the characteristics of Fbxo45-deficient mice and those of Phr1-deficient mice. Both Fbxo45- and Phr1-deficient mice die soon after birth as a result of respiratory distress and show both defective outgrowth of the phrenic nerve and impaired synaptic activity at NMJs (1, 2). Furthermore, both types of mutant mice manifest a pronounced and specific loss of axon tracts such as the anterior commissure and projections that form the internal capsule (1, 20). These observations indicate that Fbxo45 and Phr1 function in the same pathway and that not only the physical association of PAM or RPM-1 with Fbxo45 or FSN-1, respectively, but also the functional collaboration of these proteins is evolutionarily conserved.

Our study suggests that although the cellular processes that underlie axon guidance, synaptogenesis, and cell migration are fundamentally different, similar molecules may be involved. We have thus shown that Fbxo45 contributes to axon projection, synapse formation, and neuronal migration. Although

FIG. 8. Impaired neuronal migration in *Fbxo45*$^{-/-}$ spinal cord. (A to D) Structure of the spinal cord of wild-type (A and C) or *Fbxo45*$^{-/-}$ (B and D) embryos at E18.5. Transverse sections of the neck region were stained with hematoxylin-eosin. The images in panels A and B are shown at higher magnification in panels C and D, respectively. The gray matter is enlarged, distended, and flattened laterally, resulting in the loss of its invagination around the lateral column (arrowheads), in the *Fbxo45*$^{-/-}$ spinal cord. Abbreviations: DRG, dorsal root ganglion; Gm, gray matter; Wm, white matter. (E to H) Immunofluorescence staining of transverse sections of the brachial portion of wild-type (E and G) or *Fbxo45*$^{-/-}$ (F and H) embryos at E12.5 with anti-choline acetyltransferase (E and F) or with anti-Isl1 (G and H). The populations of motor neurons positive for choline acetyltransferase (ChAT) or for Isl1 form the LMC (arrows) and the MMC (arrowheads) in the wild-type spinal cord. The LMC is poorly formed, and the MMC is aberrantly distributed (asterisks) in the *Fbxo45*$^{-/-}$ spinal cord. All scale bars, 200 μm.

the molecular mechanisms responsible for the coordination of axon growth, synaptogenesis, and cell migration remain obscure, they may include regulation by protein kinases that modify the function of microtubule modulators. Such kinases include Cdk5 (38), glycogen synthase kinase 3β (16), MARK1 (MAP/microtubule affinity-regulating kinase 1), protein kinase A (6, 34), and JNK (39). Our findings that disruption of *Fbxo45* affects axon guidance, synaptogenesis, and neuronal migration support the existence of such a coordinating mechanism and provide clues for determination of its molecular basis.

ACKNOWLEDGMENTS

We thank M. Shirane, K. Yumimoto, R. Tsunematsu, and M. Nishiyama for valuable discussions; N. Nishimura, Y. Yamada, K. Takeda, and other laboratory members for technical assistance; and A. Ohta and M. Kimura for help in preparation of the manuscript.

This work was supported in part by a grant from the Ministry of Education, Culture, Sports, Science, and Technology of Japan and by a research grant from the Takeda Science Foundation.

REFERENCES

1. **Bloom, A. J., B. R. Miller, J. R. Sanes, and A. DiAntonio.** 2007. The requirement for Phr1 in CNS axon tract formation reveals the corticostriatal boundary as a choice point for cortical axons. Genes Dev. **21:**2593–2606.
2. **Burgess, R. W., K. A. Peterson, M. J. Johnson, J. J. Roix, I. C. Welsh, and T. P. O'Brien.** 2004. Evidence for a conserved function in synapse formation reveals Phr1 as a candidate gene for respiratory failure in newborn mice. Mol. Cell. Biol. **24:**1096–1105.
3. **Cardozo, T., and M. Pagano.** 2004. The SCF ubiquitin ligase: insights into a molecular machine. Nat. Rev. Mol. Cell Biol. **5:**739–751.
4. **Cenciarelli, C., D. S. Chiaur, D. Guardavaccaro, W. Parks, M. Vidal, and M. Pagano.** 1999. Identification of a family of human F-box proteins. Curr. Biol. **9:**1177–1179.
5. **Collins, C. A., Y. P. Wairkar, S. L. Johnson, and A. DiAntonio.** 2006. Highwire restrains synaptic growth by attenuating a MAP kinase signal. Neuron **51:**57–69.
6. **Drewes, G., A. Ebneth, U. Preuss, E. M. Mandelkow, and E. Mandelkow.** 1997. MARK, a novel family of protein kinases that phosphorylate microtubule-associated proteins and trigger microtubule disruption. Cell **89:**297–308.
7. **D'Souza, J., M. Hendricks, S. Le Guyader, S. Subburaju, B. Grunewald, K. Scholich, and S. Jesuthasan.** 2005. Formation of the retinotectal projection requires Esrom, an ortholog of PAM (protein associated with Myc). Development **132:**247–256.
8. **Gallo, K. A., and G. L. Johnson.** 2002. Mixed-lineage kinase control of JNK and p38 MAPK pathways. Nat. Rev. Mol. Cell Biol. **3:**663–672.
9. **Greer, J. J., D. W. Allan, M. Martin-Caraballo, and R. P. Lemke.** 1999. An overview of phrenic nerve and diaphragm muscle development in the perinatal rat. J. Appl. Physiol. **86:**779–786.
10. **Guardavaccaro, D., and M. Pagano.** 2004. Oncogenic aberrations of cullin-dependent ubiquitin ligases. Oncogene **23:**2037–2049.
11. **Guo, Q., J. Xie, C. V. Dang, E. T. Liu, and J. M. Bishop.** 1998. Identification of a large Myc-binding protein that contains RCC1-like repeats. Proc. Natl. Acad. Sci. USA **95:**9172–9177.
12. **Han, S., R. M. Witt, T. M. Santos, C. Polizzano, B. L. Sabatini, and V. Ramesh.** 2008. Pam (Protein associated with Myc) functions as an E3 ubiquitin ligase and regulates TSC/mTOR signaling. Cell. Signal. **20:**1084–1091.
13. **Hatakeyama, S., M. Kitagawa, K. Nakayama, M. Shirane, M. Matsumoto, K. Hattori, H. Higashi, H. Nakano, K. Okumura, K. Onoe, R. A. Good, and K. I. Nakayama.** 1999. Ubiquitin-dependent degradation of IκBα is mediated by a ubiquitin ligase Skp1/Cul 1/F-box protein FWD1. Proc. Natl. Acad. Sci. USA **96:**3859–3863.
14. **Hershko, A., and A. Ciechanover.** 1998. The ubiquitin system. Annu. Rev. Biochem. **67:**425–479.
15. **Hirai, S., F. Cui de, T. Miyata, M. Ogawa, H. Kiyonari, Y. Suda, S. Aizawa, Y. Banba, and S. Ohno.** 2006. The c-Jun N-terminal kinase activator dual leucine zipper kinase regulates axon growth and neuronal migration in the developing cerebral cortex. J. Neurosci. **26:**11992–12002.
16. **Jiang, H., W. Guo, X. Liang, and Y. Rao.** 2005. Both the establishment and the maintenance of neuronal polarity require active mechanisms: critical roles of GSK-3β and its upstream regulators. Cell **120:**123–135.
17. **Jin, J., T. Cardozo, R. C. Lovering, S. J. Elledge, M. Pagano, and J. W. Harper.** 2004. Systematic analysis and nomenclature of mammalian F-box proteins. Genes Dev. **18:**2573–2580.
18. **Kamura, T., K. Maenaka, S. Kotoshiba, M. Matsumoto, D. Kohda, R. C. Conaway, J. W. Conaway, and K. I. Nakayama.** 2004. VHL-box and SOCS-box domains determine binding specificity for Cul2-Rbx1 and Cul5-Rbx2 modules of ubiquitin ligases. Genes Dev. **18:**3055–3065.
19. **Lee, S. K., and S. L. Pfaff.** 2001. Transcriptional networks regulating neuronal identity in the developing spinal cord. Nat. Neurosci. **4**(Suppl.)**:**1183–1191.
20. **Lewcock, J. W., N. Genoud, K. Lettieri, and S. L. Pfaff.** 2007. The ubiquitin ligase Phr1 regulates axon outgrowth through modulation of microtubule dynamics. Neuron **56:**604–620.
21. **Liao, E. H., W. Hung, B. Abrams, and M. Zhen.** 2004. An SCF-like ubiquitin ligase complex that controls presynaptic differentiation. Nature **430:**345–350.
22. **Lopez-Bendito, G., K. Sturgess, F. Erdelyi, G. Szabo, Z. Molnar, and O. Paulsen.** 2004. Preferential origin and layer destination of GAD65-GFP cortical interneurons. Cereb. Cortex **14:**1122–1133.
23. **Marin, O., A. Yaron, A. Bagri, M. Tessier-Lavigne, and J. L. Rubenstein.** 2001. Sorting of striatal and cortical interneurons regulated by semaphorin-neuropilin interactions. Science **293:**872–875.
24. **McCabe, B. D., S. Hom, H. Aberle, R. D. Fetter, G. Marques, T. E. Haerry, H. Wan, M. B. O'Connor, C. S. Goodman, and A. P. Haghighi.** 2004. Highwire regulates presynaptic BMP signaling essential for synaptic growth. Neuron **41:**891–905.
25. **Motegi, A., J. Fujimoto, M. Kotani, H. Sakuraba, and T. Yamamoto.** 2004. ALK receptor tyrosine kinase promotes cell growth and neurite outgrowth. J. Cell Sci. **117:**3319–3329.
26. **Murthy, V., S. Han, R. L. Beauchamp, N. Smith, L. A. Haddad, N. Ito, and V. Ramesh.** 2004. Pam and its ortholog highwire interact with and may negatively regulate the TSC1.TSC2 complex. J. Biol. Chem. **279:**1351–1358.
27. **Nakata, K., B. Abrams, B. Grill, A. Goncharov, X. Huang, A. D. Chisholm, and Y. Jin.** 2005. Regulation of a DLK-1 and p38 MAP kinase pathway by the ubiquitin ligase RPM-1 is required for presynaptic development. Cell **120:**407–420.
28. **Nakayama, K., N. Ishida, M. Shirane, A. Inomata, T. Inoue, N. Shishido, I. Horii, D. Y. Loh, and K. I. Nakayama.** 1996. Mice lacking $p27^{Kip1}$ display increased body size, multiple organ hyperplasia, retinal dysplasia, and pituitary tumors. Cell **85:**707–720.
29. **Nakayama, K., H. Nagahama, Y. A. Minamishima, M. Matsumoto, I. Nakamichi, K. Kitagawa, M. Shirane, R. Tsunematsu, T. Tsukiyama, N. Ishida, M. Kitagawa, K. I. Nakayama, and S. Hatakeyama.** 2000. Targeted disruption of *Skp2* results in accumulation of cyclin E and $p27^{Kip1}$, polyploidy and centrosome overduplication. EMBO J. **19:**2069–2081.
30. **Nakayama, K. I., and K. Nakayama.** 2006. Ubiquitin ligases: cell-cycle control and cancer. Nat. Rev. Cancer **6:**369–381.
31. **Pierre, S. C., J. Hausler, K. Birod, G. Geisslinger, and K. Scholich.** 2004. PAM mediates sustained inhibition of cAMP signaling by sphingosine-1-phosphate. EMBO J. **23:**3031–3040.
32. **Sakuma, H., A. Ikeda, S. Oka, Y. Kozutsumi, J. P. Zanetta, and T. Kawasaki.** 1997. Molecular cloning and functional expression of a cDNA encoding a new member of mixed lineage protein kinase from human brain. J. Biol. Chem. **272:**28622–28629.
33. **Sanes, J. R., and J. W. Lichtman.** 1999. Development of the vertebrate neuromuscular junction. Annu. Rev. Neurosci. **22:**389–442.
34. **Schaar, B. T., K. Kinoshita, and S. K. McConnell.** 2004. Doublecortin microtubule affinity is regulated by a balance of kinase and phosphatase activity at the leading edge of migrating neurons. Neuron **41:**203–213.
35. **Schaefer, A. M., G. D. Hadwiger, and M. L. Nonet.** 2000. rpm-1, a conserved neuronal gene that regulates targeting and synaptogenesis in *C. elegans*. Neuron **26:**345–356.
36. **Shirane, M., and K. I. Nakayama.** 2006. Protrudin induces neurite formation by directional membrane trafficking. Science **314:**818–821.
37. **Shirane, M., M. Ogawa, J. Motoyama, and K. I. Nakayama.** 2008. Regulation of apoptosis and neurite extension by FKBP38 is required for neural tube formation in the mouse. Genes Cells **13:**635–651.
38. **Tanaka, T., F. F. Serneo, H. C. Tseng, A. B. Kulkarni, L. H. Tsai, and J. G. Gleeson.** 2004. Cdk5 phosphorylation of doublecortin ser297 regulates its effect on neuronal migration. Neuron **41:**215–227.
39. **Tararuk, T., N. Ostman, W. Li, B. Bjorkblom, A. Padzik, J. Zdrojewska, V. Hongisto, T. Herdegen, W. Konopka, M. J. Courtney, and E. T. Coffey.** 2006. JNK1 phosphorylation of SCG10 determines microtubule dynamics and axodendritic length. J. Cell Biol. **173:**265–277.
40. **Weissman, A. M.** 2001. Themes and variations on ubiquitylation. Nat. Rev. Mol. Cell Biol. **2:**169–178.
41. **Willmann, R., and C. Fuhrer.** 2002. Neuromuscular synaptogenesis: clustering of acetylcholine receptors revisited. Cell. Mol. Life Sci. **59:**1296–1316.
42. **Wilson, L., and M. Maden.** 2005. The mechanisms of dorsoventral patterning in the vertebrate neural tube. Dev. Biol. **282:**1–13.
43. **Wu, C., R. W. Daniels, and A. DiAntonio.** 2007. DFsn collaborates with Highwire to down-regulate the Wallenda/DLK kinase and restrain synaptic terminal growth. Neural Dev. **2:**16.
44. **Wu, C., Y. P. Wairkar, C. A. Collins, and A. DiAntonio.** 2005. Highwire function at the Drosophila neuromuscular junction: spatial, structural, and temporal requirements. J. Neurosci. **25:**9557–9566.

45. **Xu, Q., I. Cobos, E. De La Cruz, J. L. Rubenstein, and S. A. Anderson.** 2004. Origins of cortical interneuron subtypes. J. Neurosci. **24:**2612–2622.
46. **Yamanaka, A., M. Yada, H. Imaki, M. Koga, Y. Ohshima, and K. Nakayama.** 2002. Multiple Skp1-related proteins in *Caenorhabditis elegans*: diverse patterns of interaction with Cullins and F-box proteins. Curr. Biol. **12:**267–275.
47. **Yoshida, K.** 2005. Characterization of estrogen-induced F-box protein FBXO45. Oncol. Rep. **14:**531–535.
48. **Zhen, M., X. Huang, B. Bamber, and Y. Jin.** 2000. Regulation of presynaptic terminal organization by C. elegans RPM-1, a putative guanine nucleotide exchanger with a RING-H2 finger domain. Neuron **26:**331–343.
49. **Zheng, N., B. A. Schulman, L. Song, J. J. Miller, P. D. Jeffrey, P. Wang, C. Chu, D. M. Koepp, S. J. Elledge, M. Pagano, R. C. Conaway, J. W. Conaway, J. W. Harper, and N. P. Pavletich.** 2002. Structure of the Cul1-Rbx1-Skp1-F box^{Skp2} SCF ubiquitin ligase complex. Nature **416:**703–709.